Use of streamflow indices to identify the catchment drivers of hydrograph

Jeenu Mathai[1] and Pradeep P. Mujumdar[1,2]

[1]Department of Civil Engineering, Indian Institute of Science, Bangalore, India

[2]Interdisciplinary Centre for Water Research, Indian Institute of Science, Bangalore, India

Correspondence to: Pradeep. P. Mujumdar (pradeep@iisc.ac.in)

Abstract. Time irreversibility or temporal asymmetry refers to the steeper ascending and gradual descending parts of a streamflow hydrograph. The primary goal of this study is to bring out the distinction between streamflow indices directly linked with rising limbs and falling limbs and to explore ~~-~~their utility in uncovering processes associated with the steeper ascending and gradual descending limbs of the hydrograph within the time-irreversibility paradigm. Different streamflow indices are correlated with ~~-~~the rising and falling limbs and the catchment attributes. **T**he key attributes governing rising and falling limbs are then identified. The contribution of the work is on differentiating hydrographs by their time irreversibility features and offering an alternative way to recognize primary drivers of streamflow hydrographs. A series of spatial maps describing the streamflow indices and their regional variability in the Contiguous United States (CONUS) is introduced here. These indices complement the catchment attributes provided earlier (Addor et al., 2017) for the CAMELS data set. Findings of the study revealed that the elevation, fraction of precipitation falling as snow~~,~~ and depth to bedrock mainly characterize the rising limb density, whereas the aridity and frequency of precipitation influence the rising limb scale parameter. Moreover, the rising limb shape parameter is primarily influenced by forest fraction, the fraction of precipitation falling as snow, mean slope, mean elevation, sand fraction, and precipitation frequency. It is noted that falling limb density is mainly governed by climate indices, mean elevation, and the fraction of precipitation falling as snow. However, the recession coefficients are controlled by mean elevation, mean slope, clay, the fraction of precipitation falling as snow, forest fraction, and sand fraction.~~Streamflow indices are flow descriptors that quantify the streamflow dynamics, which are usually determined for a specific basin and are distinct from other basin features. The streamflow indices are appropriate for large-scale and comparative hydrology studies, independent of statistical assumptions and can distinguish signals that indicate basin behavior over time. In this paper, the characteristic features of the hydrograph's temporal asymmetry due to its different underlying hydrologic processes are primarily highlighted. Time irreversibility or temporal asymmetry refers to the steeper ascending and gradual descending parts of a streamflow hydrograph. Streamflow indices linked to each limb of the hydrograph within the time-irreversibility paradigm are distinguished with respect to its processes driving the rising and falling limbs. Various streamflow indices relating the rising and falling limbs, and the catchment attributes such as climate, topography, vegetation, geology and soil are then correlated. Finally, the key attributes governing rising and falling limbs are identified. The novelty of the work is on differentiating hydrographs by their time irreversibility property and offering an alternative way to recognize primary drivers of streamflow hydrographs. A set of streamflow indices at the catchment scale for 671 basins in the Contiguous United States (CONUS) is introduced here. These streamflow indices complement the catchment attributes provided earlier

~~(Addor et al., 2017) for the CAMELS data set. A series of spatial maps describing the streamflow indices and their regional variability over the CONUS is illustrated in this study.~~

Formatted: Font: English (United States)

1 Introduction

Hydrologists use data to understand the hydrologic system by identifying several unique catchment signatures and employ various flow descriptors independent of statistical assumptions yet capable of capturing signals that reflect the basin's long-term unique behavior. Hydrological indices, commonly referred to as hydrologic metrics, hydrologic signatures, or diagnostic signatures, are quantitative flow metrics that characterize statistical or dynamical hydrological data series (McMillan, 2021). Specifically, streamflow indices are flow descriptors derived from discharge time-series data, and a considerable collection of indices are available to aid in the better characterization of hydrological features, ranging from basic statistics like the mean to more sophisticated metrics (Addor et al., 2018; McMillan, 2021). In many cases, daily streamflow records are not permitted for redistribution; however, researchers have computed streamflow indices and made them publicly accessible.

Hydrological indices are increasingly used in emerging areas such as global-scale hydrologic modeling and large-sample hydrology to extract relevant information and compare the different watershed processes (Addor et al., 2017, 2018; McMillan, 2021). These indices offer an indirect way to explore hydrological processes as well as provide insights into hydrologic behavior in catchments where data other than streamflow is restricted and are widely used in process exploration, model calibration, model selection, and catchment classification (Addor et al., 2018; Clark et al., 2011; Kuentz et al., 2017; McMillan et al., 2011; Sawicz et al., 2011). McMillan (2021) presented a classification that differentiates between statistics and dynamics-based signatures and between signatures at different timescales.

The relevance of time irreversibility (or temporal asymmetry) of streamflow variability on a daily scale has been emphasized in recent studies (Koutsoyiannis, 2020; Mathai and Mujumdar, 2019; Serinaldi and Kilsby, 2016). The disparity in physical mechanisms driving the hydrograph's rising and falling limbs (Fig.1) contributes to time irreversibility. ~~(~~Koutsoyiannis~~,~~ (2020) shows that irreversibility may be ignored at scales relevant to hydrological applications in atmospheric processes, but it is critical to include irreversibility in studies related to streamflow. ~~Unlike other variables such as temperature, wind, precipitation, time irreversibility has been marked for streamflow at a daily scale (Koutsoyiannis, 2020).~~ Streamflow recessions convey valuable information about the basin storage properties and aquifer characteristics (Aksoy & Bayazit, 2000). High variability encountered in the recession behaviour of individual segments is always a challenge in modeling the recession limb (Tallaksen, 1995). Recessions do not follow a simple form~~,~~ due to their nonlinear nature (Aksoy et al., 2001). Various segments of recession represent different stages in the flow process and there is a need to differentiate the recession to various segments and to characterize the recession rates separately. Such segmentation of recession curves enables us to reveal the nonlinear behavior of streamflow dynamics. Time irreversibility must therefore be acknowledged in streamflow analysis, accounting for the distinction of the recession into different segments, with a faster recession induced by high discharges caused by surface runoff and a slower recession caused by baseflow (Fig.1), and the characterization of the recession rates separately (Mathai and Mujumdar, 2019). In this study, streamflow indices are chosen to better understand different hydrological processes by recognizing the streamflow

hydrograph's temporal asymmetry. The novelty in the work presented here is to differentiate hydrograph limbs by their time irreversibility property and use their associated indices to provide an approach to derive insights on the primary drivers of streamflow hydrographs.

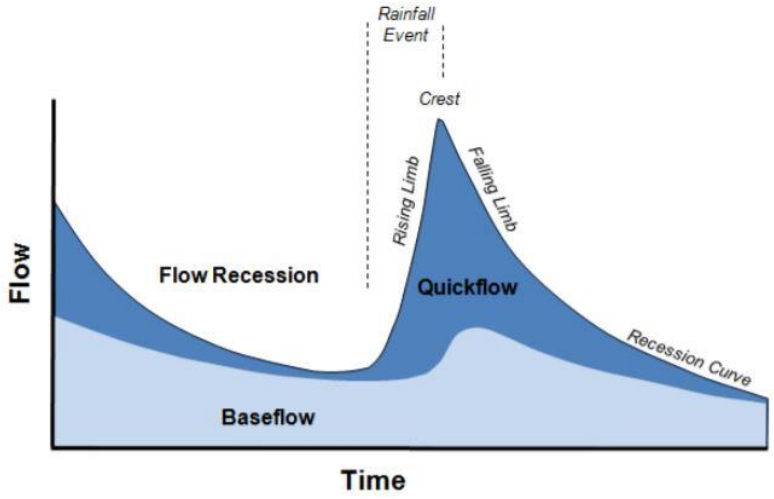

Figure 1. Schematic representation of rising limb and falling limb
(source: Environment Southland;
https://www.es.govt.nz/environment/water/groundwater/groundwater-monitoring)

The analysis employs a collection of indices drawn from hydrograph shape diagnoses, to extract information about the properties of rising and falling limbs of the hydrograph. The principle of time irreversibility is encapsulated by six streamflow indices that characterize the shape of a streamflow hydrograph.

The goals of this study are as follows: i) to identify the key drivers of streamflow hydrograph (rising and falling limbs) in terms of catchment attributes (eg. mean slope, aridity, fraction of precipitation falling as snow) using time-irreversibility-based indices; ii) to present a spatial map-based attribute class based on streamflow indices for a large-sample hydrology dataset. The attribute class is a broad classification of attributes based on a particular aspect/feature. *Topography, climate, and soil* are examples of attribute classes. In this study, we present a new attribute class of streamflow indices related to rising and falling limbs, referred to as *"TI-streamflow indices" (Time-irreversibility streamflow indices).*

Hydrograph analysis is referred to as the investigation of the numerous factors that influence hydrograph shape (Rogers, 1972). The presence of hydrographs with a similar shape in long-term observation series of runoff suggests~~demonstrates~~ that the same conditions of runoff generation reoccur from time to time in the catchment of a river due to climate cyclicity and as a result of hydrological processes (Khrystyuk et al., 2017). Because climatic factors are dynamic in space and time, they seem to be the most significant factors influencing the hydrograph shape provided that changes in catchment conditions like land use are small. Khrystyuk et al., (2017)~~.~~ suggested that for the Desna river basin in Russia, temperature, snow water equivalent, and snowmelt conditions are the most critical factors influencing the shape of hydrographs. However, it is likely that these controls may not be equally important controls on hydrograph across all regions globally. ~~Temperature, snow water equivalent, and snowmelt conditions are the most critical factors influencing the shape of hydrographs (Khrystyuk et al.,~~

2017). The shape, timing, and peak flow of a streamflow hydrograph are influenced spatially and temporally by rainfall and watershed factors (Singh, 1997). Using a physical laboratory model, a study has investigated the influence of chosen meteorological and physiographic parameters on the runoff hydrograph (Roberts and Klingeman, 1970). Storm-related parameters (rainfall intensity, rainfall duration, storm movement) and basin surface conditions are among the inputs that could be experimentally modified in the model (simulated permeability, antecedent moisture conditions). The study revealed that each variable was shown to have a substantial impact on the shape of the hydrograph (Roberts and Klingeman, 1970). Certain factors had a more considerable impact on the rising limb of the runoff hydrograph, whereas others were more important in terms of the flood crest (Roberts and Klingeman, 1970). One of the earlier studies by Roberts and Klingeman (1970) have investigated the influence of meteorological and physiographic parameters on the runoff hydrograph using a physical laboratory model. Storm-related parameters (rainfall intensity, rainfall duration, storm movement) and basin surface conditions are among the inputs that could be experimentally modified in this model. The results revealed that each of these variables mentioned above has a substantial impact on the hydrograph shape where certain factors had a more considerable effect on the rising limb of the runoff hydrograph, whereas others were more important in terms of the flood crest (Roberts and Klingeman, 1970).

As shown in numerous studies in the literature, our notion of time-irreversibility and its indices could also perform a reasonable job of articulating thehelpful in understanding the catchment drivers of streamflow hydrographs. This study presents an attribute class of hydrograph shape descriptors with temporal asymmetry. The significance of large-sample hydrology datasets in open hydrologic science and their potential to improve hydrological studies' transparency is also underlined in this study.

Large-sample hydrology (LSH) gathers information from a large number of catchments to gain a more comprehensive understanding of hydrological processes and to go beyond individual case studies. LSH helps identify catchment behavior and leads one to derive precise conclusions regarding different hydrological processes and models (Addor et al., 2020). Studies involving large-sample catchments help in understanding the drivers of hydrological change (Blöschl et al., 2019), in assessing hydrological similarity and classification (Berghuijs et al., 2014; K. A. Sawicz et al., 2014), in predictions in ungauged basins (Ehret et al., 2014), and in analysing model and data uncertainty (Coxon et al., 2014) and foster hydrology research by standardizing and automating the creation of large-sample hydrology datasets worldwide (Addor et al., 2020). LSH assists in exploring interrelationships between numerous catchment attributes related to landscape, climate, and hydrology (Addor et al., 2017; Alvarez-Garreton et al., 2018; Gupta et al., 2014; Newman et al., 2015; Sawicz et al., 2011) and generalizing rules that can significantly improve the predictability of the water cycle (Alvarez-Garreton et al., 2018).

The primary challenges in fostering LSH are data availability and accessibility, which seriously hinder its use in data-scarce regions. Despite the fact that a few large-scale hydrology studies have been undertaken, the number of publicly available large-scale datasets is still restricted (Addor et al., 2017, 2020; Coxon et al., 2020). Moreover, licensing restrictions and strict access policies make the datasets rarely available to the public (Coxon et al., 2020).

Model Parameter Estimation Experiment project (MOPEX) dataset (Duan et al., 2006), Canadian model parameter experiment (CANOPEX) database (Arsenault et al., 2016), Global Streamflow Indices and Metadata Archive (Do et al., 2018; Gudmundsson et al., 2018), Global Runoff Reconstruction (Ghiggi et al., 2019), HydroATLAS (Linke

et al., 2019) and the Catchment Attributes and MEteorology for Large-Sample studies (CAMELS) (Addor et al., 2017) are notable contributions of open and accessible large-sample catchment datasets (Coxon et al., 2020). The concept of time irreversibility-based streamflow indices is then applied to CAMELS catchments with the goal of encouraging large-sample hydrology studies. The primary contribution of this study is to establish the distinction between signatures directly linked with rising limbs and falling limbs and their utility in uncovering processes associated with the hydrograph's steeper ascending and gradual descending limbs.

2 Methods

To facilitate an understanding~~comprehension~~ of various hydrological processes and streamflow hydrograph drivers, the study employs streamflow indices considering the streamflow hydrograph's temporal asymmetry. The description of indices used in this study are tabulated in Table 1. Streamflow indices linked to each limb of the streamflow hydrograph within the time-irreversibility paradigm are distinguished since hydrographs have rising and falling limbs. The following indices are considered in the rising limb category: 1) rising limb density, 2) rising limb shape parameter, and 3) rising limb scale parameter. In contrast, 1) falling limb density 2) slope of upper recession (upper recession coefficient) 3) slope of lower recession (lower recession coefficient) are selected in falling limb category. The next step is to compute these indices for a large number of catchments and correlate them with attributes such as climate, topography, vegetation, geology, and soil. The streamflow indices can be correlated explicitly since sub-categories are involved in each of the catchment attributes discussed above. Finally, the key attributes governing rising and falling limbs can be summarized and identified. The specifics of indices are explained further below.

Rising limb density (RLD) is defined as the ratio of the number of rising limbs and the cumulative time of rising limbs (Shamir et al., 2005). RLD is a hydrograph shape descriptor without considering the flow magnitude (Fig. 2) and the expression for RLD is given as,

$$\mathrm{RLD} = \frac{\mathrm{N_{RL}}}{\mathrm{T_R}} \tag{1}$$

The ratio of the number of falling limbs to the cumulative time of falling limbs is termed as falling limb density (FLD) (Fig. 2) (Shamir et al., 2005). The expression for FLD is given as,

$$\mathrm{FLD} = \frac{\mathrm{N_{FL}}}{\mathrm{T_F}} \tag{2}$$

Table 1. Hydrological descriptors with temporal asymmetry.

Attribute		*Description*	*Unit*	*Data source*	*References*
Rising limb	RLD	Rising limb density	day^{-1}	N15 – USGS data* (https://doi.org/10.5065/D6MW2F4D)	Shamir et al. (2005)
	a	Rising limb scale parameter	-		Mathai and Mujumdar, (2019)

Formatted: Superscript

	b	Rising limb shape parameter	-		Mathai and Mujumdar, (2019)
Falling limb	FLD	Falling limb density	day^{-1}		Shamir et al. (2005)
	b_1	Upper recession coefficient	-		Mathai and Mujumdar, (2019)
	b_2	Lower recession coefficient	-		Mathai and Mujumdar, (2019)

* N15 covers 671 catchments in the contiguous USA (CONUS), which provides daily meteorological forcing and daily streamflow measurements from the United States Geological Survey (USGS).

Formatted: Font: 12 pt

$$Rising\ limb\ density = \frac{3}{\Delta T1 + \Delta T3 + \Delta T5}$$

$$Falling\ limb\ density = \frac{3}{\Delta T2 + \Delta T4 + \Delta T6}$$

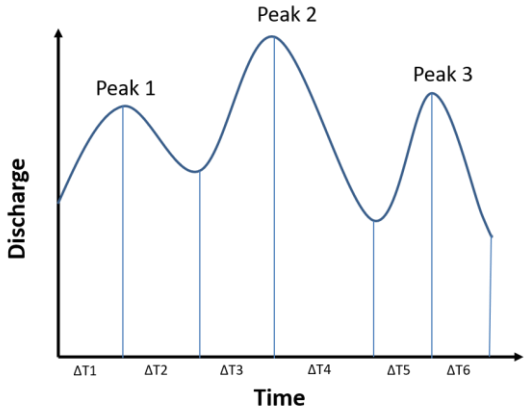

Figure 2. Schematic example of rising limb density (RLD) and falling limb density (FLD) calculation (Shamir et al., 2005).

We first identify the hydrologic state of the stream (ascension and recession) (Mathai and Mujumdar, 2019). To determine the hydrologic state of a stream - increasing (wet) or decreasing (dry) - on a given day, a time series of diurnal increments is extracted by differencing the original time series with its one-day lagged time series. The positive increments are identified as diurnal increments for wet days (ascension limb).

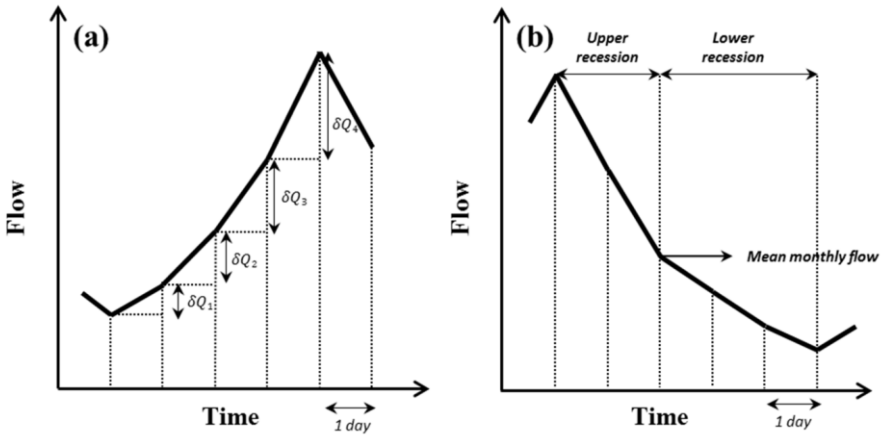

Figure 3. Schematic representation of flow series (a) ascension limb and (b) recession limb (Mathai and Mujumdar, 2019).

To characterize the shape of the rising limbs occurring on wet days, the diurnal increments are fitted using an appropriate probability density function. The Weibull distribution reflects the diurnal increments of streamflow that occur on wet days satisfactorily (Mathai and Mujumdar, 2019; Stagge and Moglen, 2013; Szilagyi et al., 2006), and the scale 'a' and shape 'b' parameters of the Weibull distribution are computed for each catchment by using observed diurnal increments of streamflow (indicating δQ) of the ascension limb (Fig 3.a). The Weibull pdf is positive only for positive values of x, and is zero otherwise. For strictly positive values of the scale parameter a and shape parameter b, the density function is given by

$$f(x;a,b) = \begin{cases} \frac{b}{a}\left(\frac{x}{a}\right)^{b-1} e^{-(x/a)^b} & x \geq 0, \\ 0 & x < 0\,, \end{cases} \quad (3)$$

where $a > 0,\ b > 0$. The shape and scale parameters of the Weibull distribution are estimated for each catchment from the observed diurnal increments of the streamflow. The scale parameter controls the magnitude of the increasing limb, whilst the shape parameter reflects the flashiness of the increasing limb. The scale parameter is related to the magnitude of storm events which mirrors the general shape of flows in the stream. As a result, correlating these parameters with catchment attributes reveals which catchment attributes drive the magnitude and flashiness of rising limbs.

In contrast, an exponential recession is used to capture the shape of the falling limbs on dry days of the daily hydrograph, representing the falling limbs' underlying dynamics (Mathai and Mujumdar, 2019). As the upper recession refers to the fast flow following a storm event and the lower recession refers to the baseflow recession, falling limb modeling is done in two stages (Fig 3.b) (Aksoy, 2003; Aksoy and Bayazit, 2000). The steps to obtain recession coefficients b_1 and b_2 are explained below (Mathai and Mujumdar, 2019). To portray the shape of the recession limbs occurring on dry days of the daily hydrograph, an exponential recession is employed to capture the falling limbs' underlying dynamics (Mathai & Mujumdar, 2019). The expression for the exponential recession is given as follows,

$$Q_t = Q_0 e^{-bt} \quad (4)$$

where b is the recession coefficient, t is time, Q_t is the flow t days after the peak and Q_0 is the peak flow (Mathai & Mujumdar, 2019). Mean flow value is chosen as an appropriate measure (Sargent, 1979) to divide the recession into two stages. The limbs with a peak flow value greater than the observed mean flow value are considered as upper recessions and those with peak flow values smaller than the observed mean as lower recessions. However, it may be noted that using the mean monthly flow can lead to unusual situations if peak flow for a given event is below the monthly mean. In such cases, the entire recession would be classified as a lower recession curve, and no upper part would exist. In those situations, there are still different driving processes for the first and second part of the recession, but these would all be lumped into one category in this case. Since we are dealing with the long-term time series, the recession slope will be nearly constant for a catchment and does not vary much with the recession separation technique used. In this study, we calculate recession slope at an annual scale. The upper recession is modelled as follows,

$$Q_t = Q_0 e^{-b_1 t} \quad (5)$$

where b_1 is the recession coefficient for the upper part of the recession limb, t is the number of days after the peak, Q_t is flow t days after the peak, Q_0 is the preceding peak flow (Mathai & Mujumdar, 2019). The lower recession is represented as,

$$Q_t = Q_0^* e^{-b_2 (t - t^*)} \quad (6)$$

where b_2 is the recession coefficient for the lower part of the recession limb, t^* is the time from the start of the lower recession, Q_0^* is the initial flow in the lower part of the recession (Mathai & Mujumdar, 2019). The recession expressions for upper and lower recession are fitted by regressing ln (Q_t/Q_0) versus t and ln (Q_t/Q_0^*) versus $t - t^*$ respectively. These linear regressions are performed on each individual recession sequence. The average of the upper/lower recession parameters is taken as the upper/lower recession parameter of that catchment (on daily time series data).

The study uses indices related to rising limb (viz., RLD, rising limb scale parameter, rising limb shape parameter) and recession limb (viz., FLD, upper recession coefficient, lower recession coefficient) to summarize the characteristic shape of steeper rising and gradually declining falling limb and its application in understanding the role of various drivers of catchment attributes in streamflow generation.

3 Dataset used

Section 3 provides the description of the dataset used and the study area chosen. This study employs the CAMELS dataset, which encompasses daily discharge data and catchment attributes for 671 catchments (Fig. 4) across the continental United States, representing a diverse set of catchments with long streamflow time series covering a wide range of hydro-climatic conditions (Addor et al., 2017). The time frame chosen for the analysis is from 1 October 1989 to 30 September 2009 (Addor et al., 2017).

The topographic characteristics of CAMELS dataset are represented in Fig. S1. Except for the Appalachian Mountains, the eastern part of the Continental United States is much flatter than the western portion, according to

mean elevation and mean slope maps (Fig. S1.a and S1.b). Figure S1.c depicts the spatial pattern of catchment size, highlighting presence of some catchments with an area greater than 10,000 km^2. The landscape of each catchment is described using multiple attributes, which can be divided into various classes as shown in Table S1 (Addor et al., 2017).

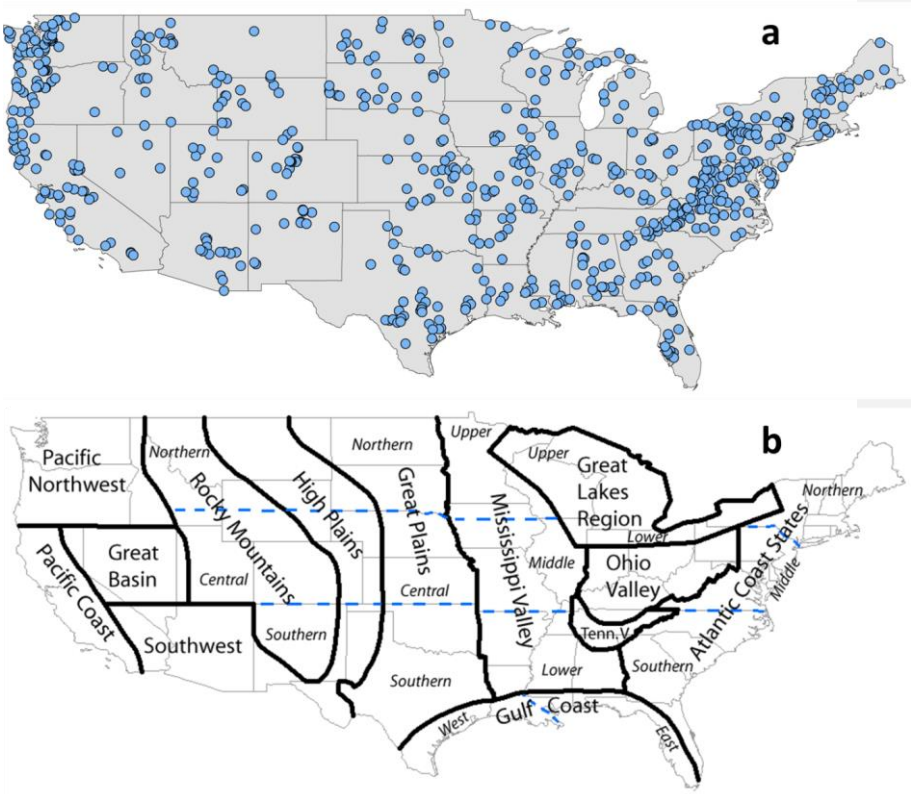

Figure 4. (a) Map of 671 CAMELS catchments in the continental United States considered in this study. (b) Geographical regions of US according to NOAA National Centers for Environmental Information referred for the analysis (source: NOAA National Centers for Environmental Information; https://www.ncdc.noaa.gov/temp-and-precip/drought/nadm/geography).

Formatted: Indent: Left: 0 cm

~~4 Results and Discussion~~

~~The first sub-section below looks at the regional variability of the streamflow indices used in this study. For the 671 CAMELS catchments, rising limb density, falling limb density, rising limb scale parameter, rising limb shape parameter, upper recession coefficient, and lower recession coefficient are computed and given as spatial maps. Streamflow indices are then presented in hydrological clusters to incorporate a more explicit spatial representation of catchment behavior across the CONUS. Catchment attributes cover a broad range of aspects of catchment hydrology such as: land cover, soil, climate, geology, topography and the association between these attributes and streamflow indices is discussed further in the subsequent section. As the climate is the most important factor in the US for the hydrological behavior for the CAMELS dataset (Jehn et al., 2020), the effect of climatic attributes on streamflow indices associated with rising and falling limbs is also investigated here.~~

~~**4.1 Spatial Variability in Streamflow Indices**~~

4 Results and Discussion

The regional variability of the streamflow indices is investigated by computing the rising limb density, falling limb density, rising limb scale parameter, rising limb shape parameter, upper recession coefficient, and lower recession coefficient for 671 CAMELS catchments and given as spatial maps. Streamflow indices are then presented in hydrological clusters to incorporate a more explicit spatial representation of catchment behavior across the CONUS. Catchment attributes cover a broad range of aspects of catchment hydrology such as: land cover, soil, climate, geology, topography and the association between these attributes and streamflow indices is discussed further in the subsequent section. It is important to understand the influence of ~~-~~climatic zones on the streamflow indices, as climate attributes influence the catchment streamflow dynamics (Addor et al., 2018; Berghuijs et al., 2014; Jehn et al., 2020; Knoben et al., 2018; Stein et al., 2021). Since the catchments are distributed in varied climatic zones (Jehn et al., 2020; Knoben et al., 2018; Stein et al., 2021), the CAMELS data is ideal for addressing this question. With this motivation, the effect of climate attributes on streamflow indices associated with rising and falling limbs is investigated here.

4.1 Spatial Variability in Streamflow Indices and Relation of the Streamflow Indices with Catchment Attributes

Streamflow indices related to rising limbs and falling limbs are computed for the selected catchments and displayed in spatial maps as shown in Fig. 5 and Fig. 6, respectively. The spatial analysis is based on the United States' geographical areas (for details, refer to Fig. ~~4~~3b) as defined by NOAA's National Centers for Environmental Information and is referred to in the following spatial maps. Furthermore, ~~ten~~ the clusters provided by Jehn et al. (2020) to represent the discrete hydrological behaviors of the continental United States are adopted in this study to understand the regional variability of catchment behavior. Figure S2 and Table S2 present the location map and details of the ten clusters. Figure S3 shows Boxplots of the catchment attributes of the clusters (after Jehn et al., 2020).

Formatted: English (India)

Even though a comprehensive dataset such as ~~-~~CAMELS provides an excellent overview of various catchments in contrasting climatic and topographic regions, it does not by itself provide insights ~~give conclusions~~ to explain hydrologic behavior. We ~~then~~ presented ~~ed~~ here streamflow indices in ~~these~~ clusters representing distinct hydrological behavior, enabling an ~~ready~~ understanding of the hydrological processes. Jehn et al. (2020) summarize the characteristics of each catchment cluster in terms of climate, hydrology and location.

The clusters presented by Jehn et al. (2020) are formed based on agglomerative hierarchical clustering with ward linkage on the principal components of the hydrological signatures. The hydrological signatures identified with the highest spatial predictability are used to cluster 643 catchments from the CAMELS dataset (Jehn et al., 2020). This facilitates straightforward interpretations of the observations to explain the hydrologic behavior in each cluster.

In this paper, we first identify the regions in the United States where high/low values of streamflow indices occur. The dominant catchment attributes of these regions are also identified using corresponding clusters. The streamflow indices and the dominant catchment attribute are then related to interpreting the obtained findings' process. ~~Features of the 10 clusters provided by Jehn et al. (2020) are used to interpret the findings of the results. Even though a comprehensive dataset like CAMELS provides an excellent overview of various catchments in contrasting climatic and topographic regions, it does not give conclusions to explain hydrologic behavior. In order to address this difficulty, we transformed the streamflow indices and presented them in clusters that represent distinct hydrological behavior which facilitates a ready interpretation of hydrological processes. The ten clusters represent groups of catchments with distinct hydrological behavior and have distinct spatial patterns as well. The clusters presented by Jehn et al. (2020) are formed based on agglomerative hierarchical clustering with ward linkage on the principal components of the hydrological signatures. The hydrological signatures that are identified with the highest spatial predictability are used to cluster 643 catchments from the CAMELS dataset.~~ In terms of geographical regions, the rising limb density is highest over the Atlantic coast states, Ohio valley, Lower Mississippi Valley, Southern Great Plains, Southwest and Pacific, and lowest along the Upper Great Lakes region, Upper Mississippi Valley, Great Basin, and Northern Rocky Mountains, Northern Interior Plains, and East of Gulf Coast (Fig. 5.a). Further, in terms of hydrological clusters, the Appalachian Mountains (Cluster 10), Southeastern and Central Plains (Cluster 1), and all Southern most states of the US (Cluster 9) witness high rising limb densities (Fig. 6.a). Cluster 1 is characterized by dense vegetation cover and low elevation resulting in little annual snowfall. Cluster 10 catchments are located in the Appalachian Mountains, with a higher mean elevation than most other clusters, experiencing low aridity and high forest cover. However, Cluster 9 encompasses all of the United States' southern states, with lower precipitation seasonality and higher forest cover and green vegetation. Furthermore, all of the catchments in Cluster 9 are very near the sea, with a low snow component and high evapotranspiration. We used Spearman rank correlation for the correlation analysis (Table 2). Green-colored coefficients represent positive correlation, and the red-colored correlation coefficients represent negative correlation (Table 2). It can be seen that the rising limb density shows a negative correlation (Table 2) with the area ($r = -0.30$), elevation ($r = -0.20$) fraction of precipitation falling as snow ($r = -0.33$), and depth to bedrock ($r = -0.32$). Northwestern Forested Mountains (Clusters 3, 4), located in the mountains of the western US, experience low values of rising limb density. The catchments of Cluster 3 have the largest snow storage in the dataset. Cluster 4 is found in the western United States' mountains, where there is a lot of snow, same as Cluster 3. Low values of rising limb density are observed due to a negative correlation with the fraction of precipitation falling as snow ($r = -0.33$). The study indicates that rising limb density is mainly governed by elevation and fraction of precipitation falling as snow in the CONUS.

Considerably low values of rising limb scale parameters are experienced over the Rocky Mountains, High Plains, Great Plains, Upper Mississippi Valley, Great Basin, Southwest, and the Great Lakes regions, whereas the Pacific

Northwest shows high values of rising limb scale parameters (Fig. 5.b). Clusters (5, 7) over the Northwestern Forested Mountains of CONUS experience very high values of rising limb scale parameters (Fig. 6.b). These catchments have the highest discharge, especially in the early summer, due to a combination of high precipitation and snowmelt. Further, the region in the Continental US which receives the highest precipitation is included in Cluster 5. Moreover, Cluster 5 consists of a large proportion of forest. Again, Cluster 7 with high values of rising limb scale parameter is characterized by high fraction of precipitation falling as snow. High precipitation and snowmelt might result in a large discharge. Higher discharges can create higher values of rising scale parameters as the rising limb scale parameter regulates the magnitude of the rising limb. Low values of rising limb scale parameters are shown by Clusters 2, 8, 9. This is because of low water availability, low snow fraction precipitation falling as snow, and high evaporation experienced in these regions. Low discharge and thus lower rising limb scale parameters can be caused by excessive evaporation, low water availability, and a low snow fraction of precipitation falling as snow. It is observed that the rising limb scale parameter (Table 2) shows a negative correlation with climate (r = -0.53 for aridity) and a positive association with the vegetation attributes (r = 0.46 for forest fraction, r = 0.41 for LAI maximum, r = 0.44 for green vegetation fraction maximum). Frequency of precipitation (r = -0.56 for high precipitation frequency, r = -0.63 for low precipitation frequency) display a strong negative association with the rising limb scale parameter.

Low rising limb shape parameter occurs along the Great Plains, Mississippi Valley, Pacific coast, and the west of Gulf Coast (Fig. 5.c). In contrast, the shape parameter over the Rocky Mountains, High Plains, Great Basin, Pacific Northwest, and the Great Lakes region witnesses the highest values of rising limb shape parameters (Fig. 5.c). All the catchments located in the Southern states of the US (Cluster 9), Great Plains and North American deserts (Cluster 8), and the Central Plains (Cluster 2) characterize low values of rising limb shape parameters (Fig. 6.c). This is due to low water availability, low snow fraction precipitation falling as snow, low leaf area index, and high evaporation experienced in these regions. Excessive evaporation and a low snow fraction of precipitation falling as snow can contribute to low discharge and thus lower rising limb shape parameters. It is noted that the rising limb shape parameter indicates (Table 2) a positive correlation with vegetation attributes (r = 0.41 for forest fraction) and the fraction of precipitation falling as snow (r = 0.53), mean slope (r = 0.36), mean elevation (r = 0.41), and sand fraction (r = 0.37) whereas, it negatively correlates with precipitation frequency (r= -0.42 for high precipitation frequency and r = -0.45 for low precipitation frequency). High values of rising limb shape parameters are seen in Clusters 3, 4 (Fig. 6.c) located in the Northwestern Forested Mountains of the western US, dominant with a summer peak of discharge caused by rapid snowmelt. The rapid snowmelt can cause flashy hydrographs with high values of rising limb shape parameters.

Catchments with a high falling limb density are predominantly located along the Great Basin and the Rocky Mountains and in the High Plains region (Fig. 7.a). This is due to less forest cover in these arid regions and falling limb density shows a positive association with the arid climate (r = 0.39). Clusters 6, 7 over Marine West Coast Forests and Western Cordillera experience smaller falling limb densities (Fig. 8.a). We can see that falling limb density is mainly governed by climate indices and is negatively correlated with the land cover characteristics (for LAI maximum (r = -0.37) and green veg frac max (r = -0.40, Table 2). Mean elevation (r = 0.55) also strongly characterizes the nature of the falling limb density. Besides, fraction of precipitation falling as snow (r = 0.42) is also positively correlated with falling limb density.

Similarities exist between the patterns of the upper recession coefficient and the lower recession coefficient (Fig. 7.b and Fig. 7.c). Clusters 3, 4 located in the Northwestern Forested Mountains, which have overall low discharge, show low values of upper and lower recession coefficients (Fig. 8.b and Fig. 8.c). Clusters 2 and 9, located in the eastern US, witness high values of recession coefficients; due to low slope inclinations, water takes a long time to reach the outlet (Fig. 8.b and Fig. 8.c). Recession coefficients are negatively correlated (Table 2) with topographic indices (with mean elevation: upper_r = -0.40, lower_r = -0.35; with mean slope: upper_r = -0.38, lower_r = -0.37, where upper_r and lower_r corresponds to correlation values of upper and lower recession coefficients respectively). Further, the recession coefficients show a positive correlation with clay (upper_r = 0.52, lower_r = 0.32) and negative correlations with the fraction of precipitation falling as snow (upper_r = -0.46, lower_r = -0.39), forest fraction (upper_r = -0.31, lower_r = -0.28), and sand fraction (upper_r = -0.38, lower_r = -0.23). Moreover, the geology attributes such as subsurface porosity (upper_r = 0.13, lower_r = 0.16) reveal a positive correlation to recession coefficients and a negative (upper_r = -0.09, lower_r = -0.18) with subsurface permeability (Table 2).

~~We first identify the regions in the United States where high/low values of streamflow indices occur. The dominant catchment attributes of these regions are also identified using corresponding clusters. The streamflow indices and the dominant catchment attribute are then related to interpret the process behind the obtained findings. In terms of geographical regions, the rising limb density is highest over the Atlantic coast states, Ohio valley, Lower Mississippi Valley, Southern Great Plains, Southwest and Pacific, and lowest along the Upper Great Lakes region, Upper Mississippi Valley, Great Basin, and Northern Rocky Mountains, Northern Interior Plains, and East of Gulf Coast (Fig. 5.a). Further, in terms of hydrological clusters, Appalachian Mountains (Cluster 10), Southeastern and Central Plains (Cluster 1) and all Southern most states of the US (Cluster 9) witness high rising limb densities and these clusters are characterized by a high forest fraction, low aridity, and high frequency of high precipitation events (Jehn et al., 2020), respectively (Fig. 6.a). The higher the forest proportion, the more precipitation is intercepted, resulting in a shallow rising limb and longer lag time of hydrograph. A high frequency of high precipitation episodes, on the other hand, can result in more rising limbs and higher rising limb densities.~~

~~Northwestern Forested Mountains (Clusters 3, 4), located in the mountains of the western US, experience low values of rising limb density as these clusters are characterized by a dominant summer peak of discharge caused by rapid snowmelt (Fig. 6.a). In these clusters, we identified regions with low rising limb densities and the main catchment characteristics as dominant summer discharge peaks induced by quick snowmelt (Jehn et al., 2020). A long lag time and shallow rising limb might be caused by snow on the ground; hence low values of rising limbs might be caused by a longer lag time.~~

~~Considerably low values of rising limb scale parameters are experienced over the Rocky Mountains, High Plains, Great Plains, Upper Mississippi Valley, Great Basin, Southwest, and the Great Lakes regions, whereas the Pacific Northwest shows high values of rising limb scale parameters (Fig. 5.b). Clusters (5, 7) over the Northwestern Forested Mountains of CONUS experience very high values of rising limb scale parameters (Fig. 6.b). These catchments have the highest discharge, especially in the early summer, due to a combination of high precipitation and snowmelt. Further, the region in the Continental US which receives the highest precipitation is included in Cluster 5. Moreover, Cluster 5 consists of a large proportion of forest. Again, Cluster 7 with high values of rising limb scale parameter is characterized by high fraction of precipitation falling as snow. High precipitation and~~

snowmelt might result in a large discharge. Higher discharges can create higher values of rising scale parameters as the rising limb scale parameter regulates the magnitude of the rising limb. Low values of rising limb scale parameters are shown by Clusters 2, 8, 9. This is because of low water availability, low snow fraction precipitation falling as snow, and high evaporation experienced in these regions. Low discharge and thus lower rising limb scale parameters can be caused by excessive evaporation, low water availability, and a low snow fraction of precipitation falling as snow.

Low rising limb shape parameter occurs along the Great Plains, Mississippi Valley, Pacific coast, and the west of Gulf Coast (Fig. 5.c). In contrast, the shape parameter over the Rocky Mountains, High Plains, Great Basin, Pacific Northwest, and the Great Lakes region witnesses the highest values of rising limb shape parameters (Fig. 5.c). All the catchments located in the Southern states of the US (Cluster 9), Great Plains and North American deserts (Cluster 8), and the Central Plains (Cluster 2) characterize low values of rising limb shape parameters (Fig. 6.c). This is due to low water availability, low snow fraction precipitation falling as snow, low leaf area index, and high evaporation experienced in these regions. Excessive evaporation and a low snow fraction of precipitation falling as snow can contribute to low discharge and thus lower rising limb shape parameters. High values of rising limb shape parameters are seen in Clusters 3, 4 (Fig. 6.c) located in the Northwestern Forested Mountains of the western US, dominant with a summer peak of discharge caused by rapid snowmelt. The rapid snowmelt can cause flashy hydrographs with high values of rising limb shape parameters.

Catchments with a high falling limb density are predominantly located along the Great Basin and the Rocky Mountains and in the High Plains region (Fig. 7.a). Clusters 4, 2, 8 over Northwestern Forested Mountains, Central Plains, Great Plains, and North American deserts characterize higher magnitudes of falling limb density, and Clusters 6, 7 over Marine West Coast Forests and Western Cordillera smaller falling limb densities (Fig. 8.a). This is due to less presence of forest cover in these arid regions and falling limb density shows a positive association with the arid climate.

Similarities exist between the patterns of the upper recession coefficient and the lower recession coefficient (Fig. 7.b and Fig. 7.c). Clusters 3, 4 located in the Northwestern Forested Mountains, which have overall low discharge, show low values of upper and lower recession coefficients (Fig. 8.b and Fig. 8.c). Clusters 2 and 9, located in the eastern US, witness high values of recession coefficients; due to low slope inclinations, water takes a long time to reach the outlet (Fig. 8.b and Fig. 8.c).

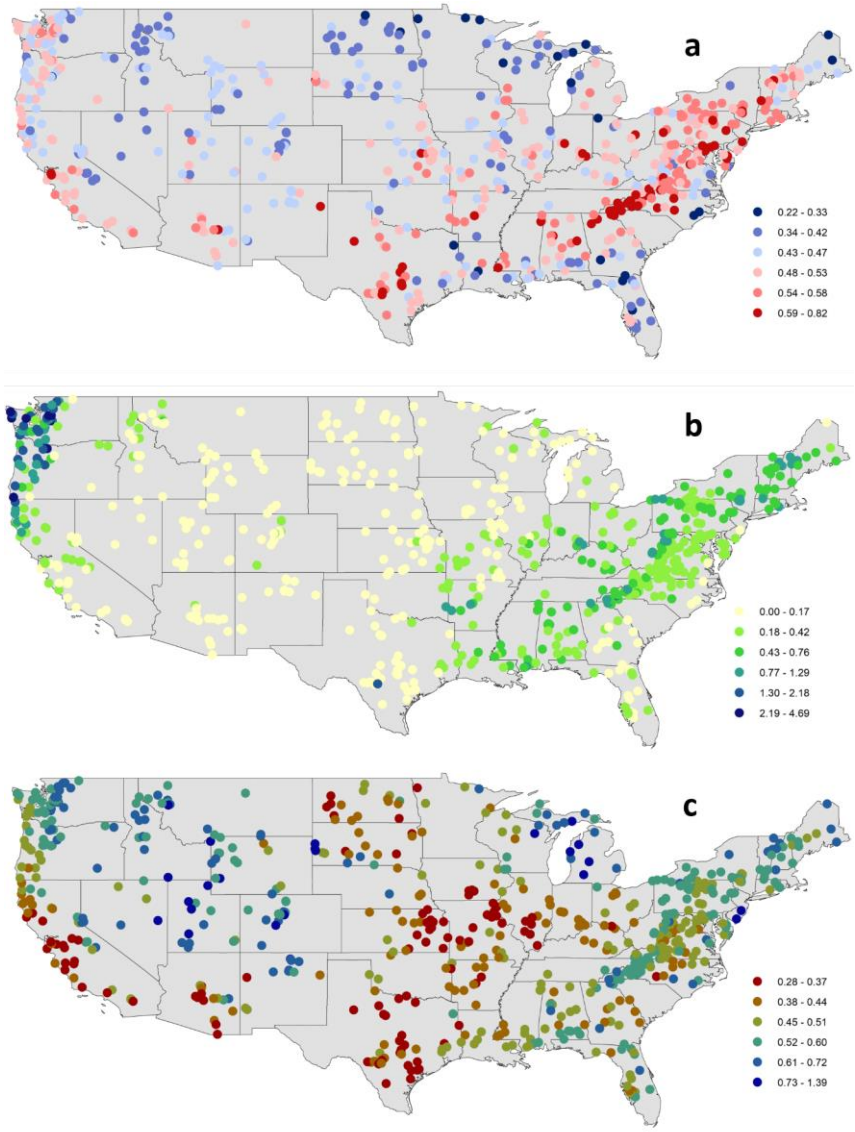

434

435 **Figure 5.** Spatial maps of streamflow indices associated with a rising limb (a) rising limb density [day^{-1}], (b)
436 rising limb scale parameter, (c) rising limb shape parameter over the CONUS**.**

437

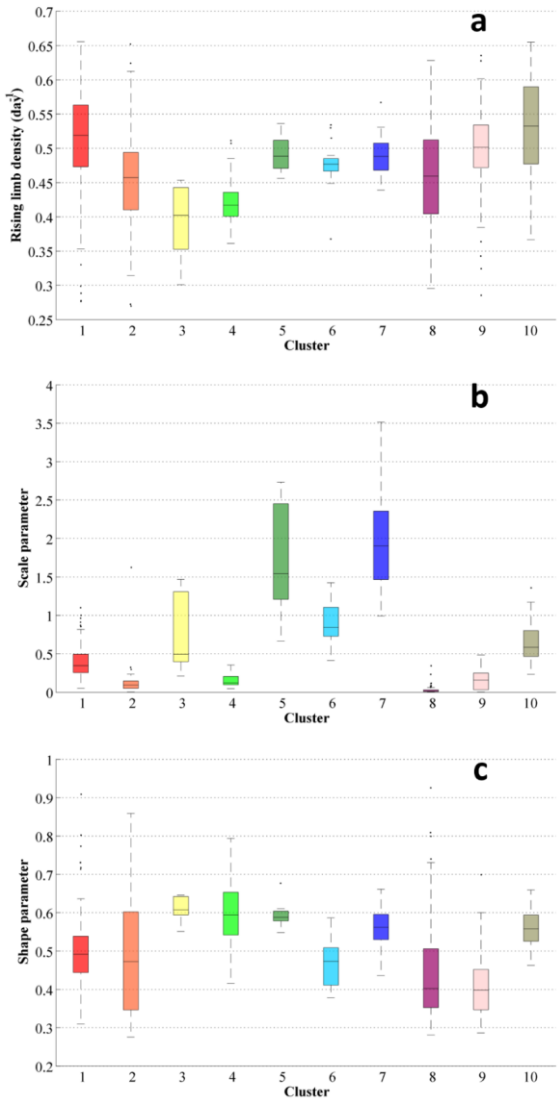

438

439 **Figure 6.** Boxplots of the hydrological descriptors linked with the rising limb (a) rising limb density [day^{-1}], (b)
440 rising limb scale parameter, (c) rising limb shape parameter of the clusters over the CONUS.

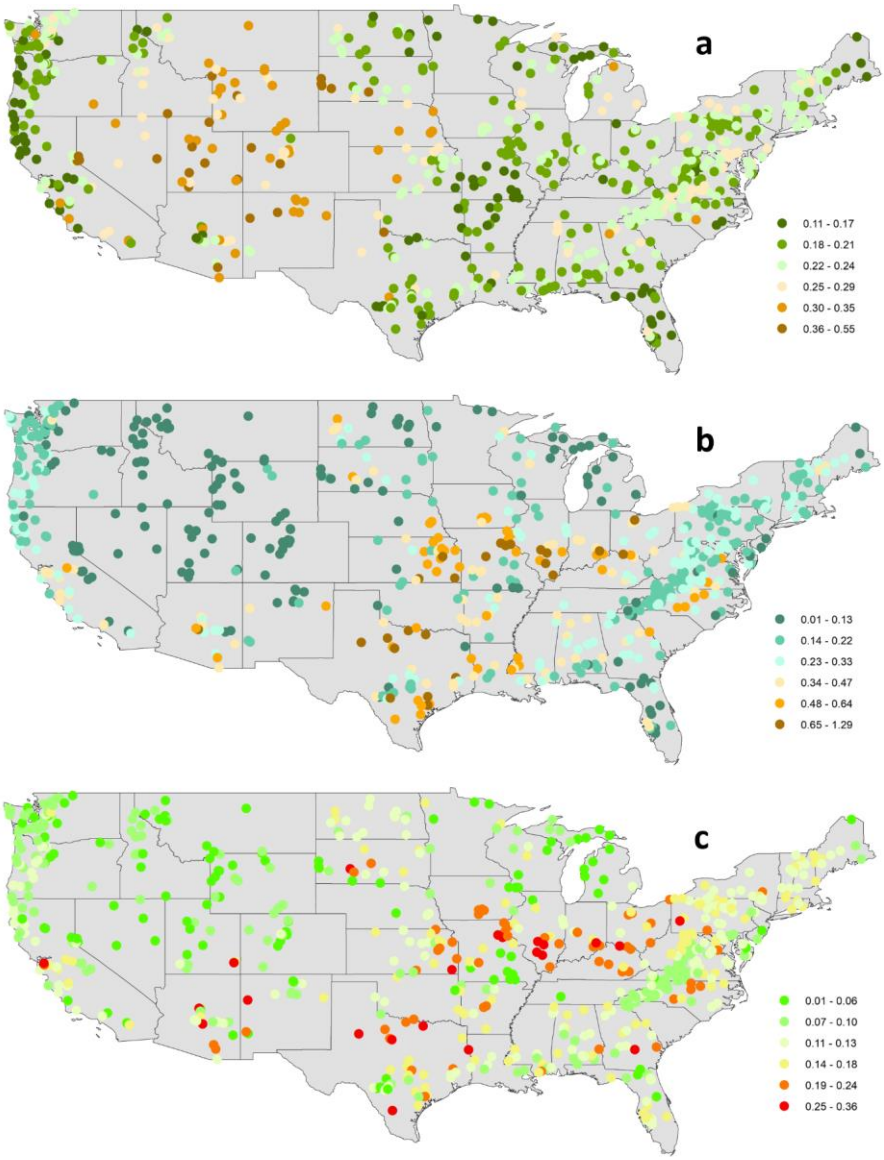

441

442 **Figure 7.** Regional variability of streamflow indices associated with the falling limb (a) falling limb density [day^{-1}], (b) upper recession coefficient, (c) lower recession coefficient over the CONUS.

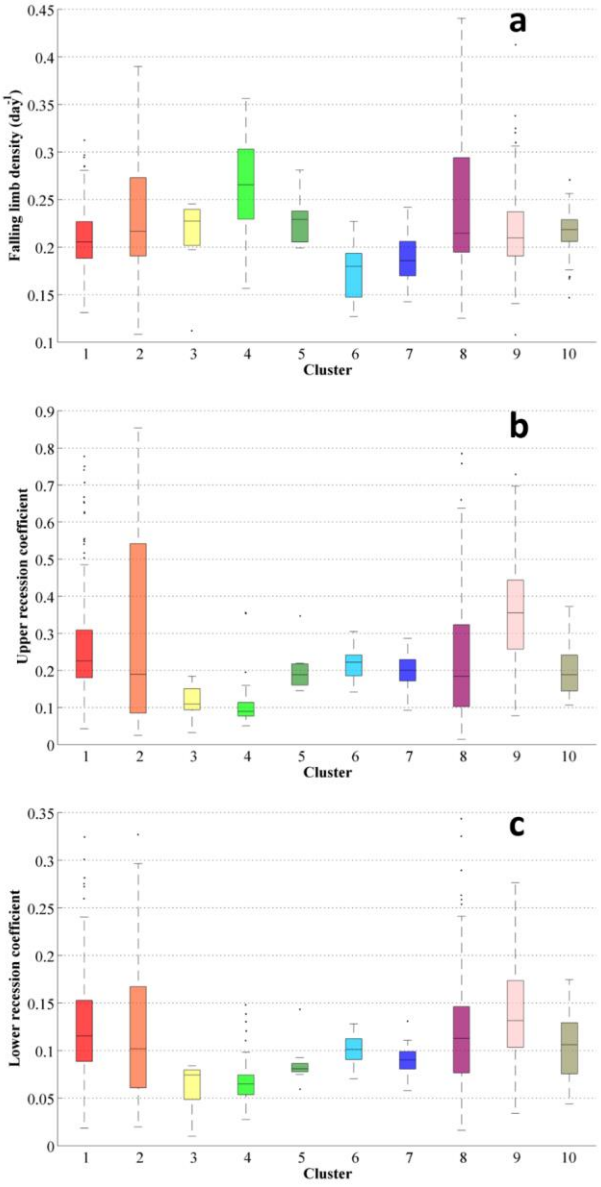

444

445 **Figure 8.** Boxplots of the streamflow indices related with the falling limb (a) falling limb density [day^{-1}], (b) upper
446 recession coefficient, (c) lower recession coefficient of the clusters.

447

448

Table 2 Correlation (r- values) between streamflow indices and the catchment attributes. Green colored coefficients represent positive correlation, and the red-colored correlation coefficients represent the negative correlation. Corresponding (*p*- values) are shown in brackets. Insignificant correlations (p > 0.05) are marked yellow.

r- value	Rising limb density	Scale parameter	Shape parameter	Falling limb density	Upper recession coefficient	Lower recession coefficient
Area	-0.30	-0.17	-0.06	-0.13	-0.06	-0.06
	(0.00)	(0.00)	(0.11)	(0.00)	(0.10)	(0.11)
Mean elevation	-0.20	-0.13	0.41	0.55	-0.40	-0.35
	(0.00)	(0.00)	(0.00)	(0.00)	(0.00)	(0.00)
Mean slope	-0.06	0.35	0.36	0.18	-0.38	-0.37
	(0.13)	(0.00)	(0.00)	(0.00)	(0.00)	(0.00)
Precipitation seasonality	-0.04	-0.36	-0.14	0.01	0.17	0.22
	(0.26)	(0.00)	(0.00)	(0.75)	(0.00)	(0.00)
Frac of precp as snow	-0.33	-0.04	0.53	0.42	-0.46	-0.39
	(0.00)	(0.27)	(0.00)	(0.00)	(0.00)	(0.00)
Aridity	-0.10	-0.53	-0.16	0.39	0.04	0.03
	(0.01)	(0.00)	(0.00)	(0.00)	(0.30)	(0.45)
High precp freq	0.08	-0.56	-0.42	0.12	0.31	0.27
	(0.04)	(0.00)	(0.00)	(0.00)	(0.00)	(0.00)
High precp dur	-0.15	0.00	-0.07	0.12	-0.11	-0.17
	(0.00)	(0.97)	(0.09)	(0.00)	(0.01)	(0.00)
Low precp freq	0.00	-0.63	-0.45	0.17	0.26	0.19
	(0.91)	(0.00)	(0.00)	(0.00)	(0.00)	(0.00)
Low precp dur	-0.03	-0.25	-0.29	0.11	0.07	0.01
	(0.49)	(0.00)	(0.00)	(0.00)	(0.07)	(0.84)
Depth to bedrock	-0.32	-0.21	-0.16	-0.19	0.19	0.21
	(0.00)	(0.00)	(0.00)	(0.00)	(0.00)	(0.00)
Sand frac	-0.28	-0.02	0.37	-0.02	-0.38	-0.23
	(0.00)	(0.62)	(0.00)	(0.63)	(0.00)	(0.00)
Clay frac	0.26	-0.15	-0.47	0.00	0.52	0.32
	(0.00)	(0.00)	(0.00)	(0.93)	(0.00)	(0.00)
Forest frac	0.10	0.46	0.41	-0.17	-0.31	-0.28
	(0.01)	(0.00)	(0.00)	(0.00)	(0.00)	(0.00)
LAI maximum	0.20	0.41	0.17	-0.37	-0.09	-0.04
	(0.00)	(0.00)	(0.00)	(0.00)	(0.03)	(0.28)
Green veg frac max	0.18	0.44	0.15	-0.40	-0.05	-0.01
	(0.00)	(0.00)	(0.00)	(0.00)	(0.16)	(0.74)
Subsurface porosity	-0.16	-0.06	-0.16	-0.08	0.13	0.16
	(0.00)	(0.12)	(0.00)	(0.03)	(0.00)	(0.00)
Subsurface permeability	-0.11	-0.04	0.06	0.03	-0.09	-0.18
	(0.00)	(0.34)	(0.12)	(0.39)	(0.02)	(0.00)
r- value	Rising limb density	Scale parameter	Shape parameter	Falling limb density	Upper recession coefficient	Lower recession coefficient

Formatted ...

Area	-0.30 **(0.00)**	-0.17 **(0.00)**	-0.06 **(0.11)**	-0.13 **(0.00)**	-0.06 **(0.10)**	-0.06 **(0.11)**
Mean elevation	-0.20 **(0.00)**	-0.13 **(0.00)**	0.41 **(0.00)**	0.55 **(0.00)**	-0.40 **(0.00)**	-0.35 **(0.00)**
Mean slope	-0.06 **(0.13)**	0.35 **(0.00)**	0.36 **(0.00)**	0.18 **(0.00)**	-0.38 **(0.00)**	-0.37 **(0.00)**
Precipitation seasonality	-0.04 **(0.26)**	-0.36 **(0.00)**	-0.14 **(0.00)**	0.01 **(0.75)**	0.17 **(0.00)**	0.22 **(0.00)**
Frac of precp as snow	-0.33 **(0.00)**	-0.04 **(0.27)**	0.53 **(0.00)**	0.42 **(0.00)**	-0.46 **(0.00)**	-0.39 **(0.00)**
Aridity	-0.10 **(0.01)**	-0.53 **(0.00)**	-0.16 **(0.00)**	0.39 **(0.00)**	0.04 **(0.30)**	0.03 **(0.45)**
High precp freq	0.08 **(0.04)**	-0.56 **(0.00)**	-0.42 **(0.00)**	0.12 **(0.00)**	0.31 **(0.00)**	0.27 **(0.00)**
High precp dur	-0.15 **(0.00)**	0.00 **(0.97)**	-0.07 **(0.09)**	0.12 **(0.00)**	-0.11 **(0.01)**	-0.17 **(0.00)**
Low precp freq	0.00 **(0.91)**	-0.63 **(0.00)**	-0.45 **(0.00)**	0.17 **(0.00)**	0.26 **(0.00)**	0.19 **(0.00)**
Low precp dur	-0.03 **(0.49)**	-0.25 **(0.00)**	-0.29 **(0.00)**	0.11 **(0.00)**	0.07 **(0.07)**	0.01 **(0.84)**
Depth to bedrock	-0.32 **(0.00)**	-0.21 **(0.00)**	-0.16 **(0.00)**	-0.19 **(0.00)**	0.19 **(0.00)**	0.21 **(0.00)**
Sand frac	-0.28 **(0.00)**	-0.02 **(0.62)**	0.37 **(0.00)**	-0.02 **(0.63)**	-0.38 **(0.00)**	-0.23 **(0.00)**
Clay frac	0.26 **(0.00)**	-0.15 **(0.00)**	-0.47 **(0.00)**	0.00 **(0.93)**	0.52 **(0.00)**	0.32 **(0.00)**
Forest frac	0.10 **(0.01)**	0.46 **(0.00)**	0.41 **(0.00)**	-0.17 **(0.00)**	-0.31 **(0.00)**	-0.28 **(0.00)**
LAI maximum	0.20 **(0.00)**	0.41 **(0.00)**	0.17 **(0.00)**	-0.37 **(0.00)**	-0.09 **(0.03)**	-0.04 **(0.28)**
Green veg frac max	0.18 **(0.00)**	0.44 **(0.00)**	0.15 **(0.00)**	-0.40 **(0.00)**	-0.05 **(0.16)**	-0.01 **(0.74)**
Subsurface porosity	-0.16 **(0.00)**	-0.06 **(0.12)**	-0.16 **(0.00)**	-0.08 **(0.03)**	0.13 **(0.00)**	0.16 **(0.00)**
Subsurface permeability	-0.11 **(0.00)**	-0.04 **(0.34)**	0.06 **(0.12)**	0.03 **(0.39)**	-0.09 **(0.02)**	-0.18 **(0.00)**

453

-

Formatted: Normal (Web), Space Before: 0 pt, After: 0 pt, Line spacing: single, Adjust space between Latin and Asian text, Adjust space between Asian text and numbers

4.2 Relation of the Streamflow Indices and the Catchment Attributes

The association between the streamflow indices related to rising and falling limbs and catchment attributes is examined in this section. Table 2 shows the relation of streamflow indices linked with rising limb, and Table 3 shows the association of indices of the falling limb with catchment attributes. We used Spearman rank correlation for the correlation analysis. (in Tables 2 and 3). Green-colored coefficients represent positive correlation, and the red-colored correlation coefficients represent negative correlation. Table 2 and Table 3 have certain columns that are blank because only significant correlation values are provided in the table. Across all five attribute classes, the vegetation/land cover attributes positively correlate with all rising limb indices (Table 2). It can be seen that the rising limb density shows a positive correlation with all the three vegetation density indicators, namely fraction of forest, maximum leaf area index, maximum green vegetation fraction (Table 2).

However, it is observed that the rising limb scale parameter shows a negative correlation with climate and a positive association with the vegetation attributes (Table 2). Aridity and frequency of precipitation (Table 2) display a strong negative association with the rising limb scale parameter. It is noted that the rising limb shape parameter indicates a positive correlation with vegetation attributes and the fraction of precipitation falling as snow, mean slope, mean elevation, and sand fraction whereas, it negatively correlates with precipitation frequency.

Falling limb density is mainly governed by climate indices and is negatively correlated with the land cover characteristics (Table 3). Mean elevation also strongly characterizes the nature of the falling limb density. Besides, aridity and fraction of precipitation falling as snow are also positively correlated with falling limb density. Recession coefficients are negatively correlated with topographic indices (Table 3). Further, the recession coefficients show a positive correlation with clay and negative correlations with the fraction of precipitation falling as snow, forest fraction, and sand fraction. Moreover, the geology attributes such as subsurface porosity reveal a positive correlation to recession coefficients and a negative with subsurface permeability (Table 3).

Table 2. Correlation between streamflow indices linked with rising limb and the catchment attributes. Green colored coefficients represent positive correlation, and the red colored correlation coefficients represent the negative correlation.

Spearman rank correlation coefficients	Topography			Climate							Soil			Land cover			Geology	
	Area	Mean elevation	Mean slope	Precipitation seasonality	Frac of precp as snow	Aridity	High precp freq	High precp dur	Low precp freq	Low precp dur	Depth to bedrock	Sand frac	Clay frac	Forest frac	LAI maximum	Green veg frac max	Subsurface porosity	Subsurface permeability
Rising limb density	-0.30	-0.20			-0.33	-0.10	0.08	-0.15			-0.32	-0.28	0.26	0.10	0.20	0.18	-0.16	-0.11
Scale parameter	-0.17	-0.13	0.35	-0.36		-0.53	-0.56		-0.63	-0.25	-0.21		-0.15	0.46	0.41	0.44		
Shape parameter		0.41	0.36	-0.14	0.53	-0.16	-0.42		-0.45	-0.29	-0.16	0.37	-0.47	0.41	0.17	0.15	-0.16	

Table 3. Correlation between streamflow indices linked with falling limb and the catchment attributes. Green colored coefficients represent positive correlation, and the red colored correlation coefficients represent the negative correlation.

Spearman rank correlation coefficients	Topography			Climate							Soil			Land cover			Geology	
	Area	Mean elevation	Mean slope	Precipitation seasonality	Frac of precp as snow	Aridity	High precp freq	High precp dur	Low precp freq	Low precp dur	Depth to bedrock	Sand frac	Clay frac	Forest frac	LAI maximum	Green veg frac max	Subsurface porosity	Subsurface permeability
Falling limb density	-0.13	0.55	0.18		0.42	0.39	0.12	0.12	0.17	0.11	-0.19			-0.17	-0.37	-0.40	-0.08	
Upper recession coefficient		-0.40	-0.38	0.17	-0.46		0.31	-0.11	0.26		0.19	-0.38	0.52	-0.31	-0.09		0.13	-0.09
Lower recession coefficient		-0.35	-0.37	0.22	-0.39		0.27	-0.17	0.19		0.21	-0.23	0.32	-0.28			0.16	-0.18

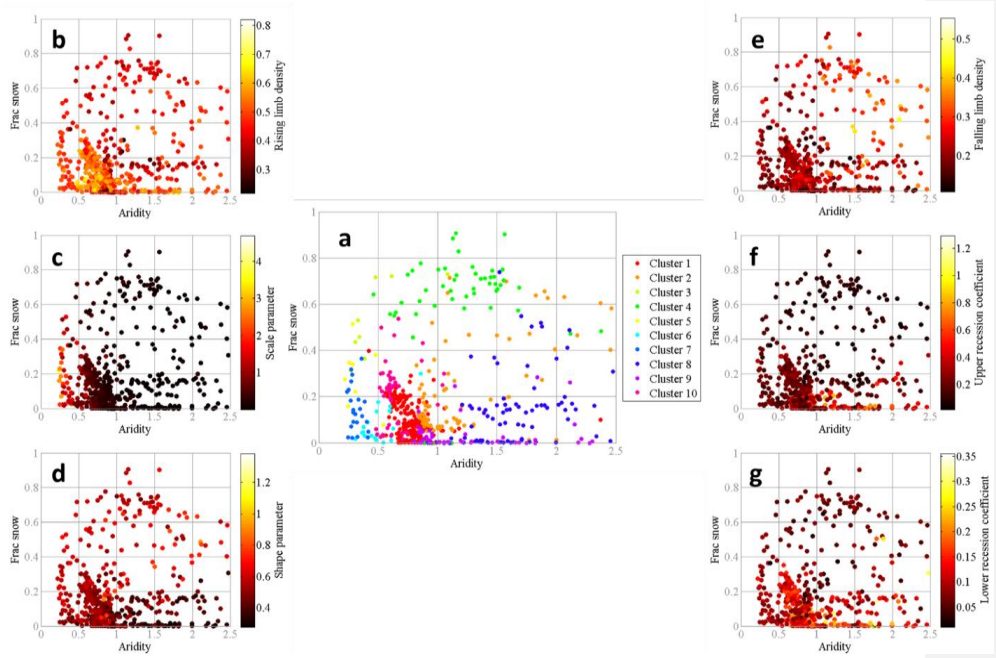

493

494 **Figure 9.** (a) Comparison of the hydrological clusters of Jehn et al. (2020) with the climate index space (fraction
495 of precipitation falling as snow vs. aridity). Single dots show the catchments and are colored by their hydrological
496 clusters. Comparison of the streamflow indices in climate index space (b) rising limb density (c) rising limb scale
497 parameter, (d) rising limb shape parameter, (e) falling limb density, (f) upper recession coefficient, (g) lower
498 recession coefficient for all catchments. Single dots show the catchments and are colored according to the value
499 of the streamflow indices.

500

501 ~~**4.3 Influence of Attributes of Climate to Streamflow Indices**~~

502 ~~The climatic indices indicate a more substantial influence on hydrological signatures than the topographic, soil,~~
503 ~~land cover, and geological attributes combined (Addor et al., 2018). Additionally, the findings of Jehn et al. (2020)~~
504 ~~highlighted that the climate appears to be the most critical factor influencing hydrological behavior in the~~
505 ~~CAMELS dataset as a whole, and depending on the location, either aridity, snow, or seasonality are most~~
506 ~~important. Hence, the streamflow indices are then examined in the climate index space (aridity along x-axis and~~
507 ~~fraction of precipitation falling as snow along the y-axis) to evaluate the main drivers of the catchments. Single~~
508 ~~dots show the catchments and are colored by their hydrological clusters (Fig. 9.a).~~

509 ~~Clusters 5, 6, 7, 1, 10 are characterized by a low fraction of precipitation falling as snow and humid climate,~~
510 ~~whereas Clusters 3, 4 have humid climate experiencing a high fraction of precipitation falling as snow (Fig. 9.a).~~
511 ~~Clusters 2, 8, 9 are featured by a low fraction of precipitation falling as snow and arid climate (Fig. 9.a). The three~~
512 ~~categories mentioned above are referred to as G1, G2, and G3, respectively.~~

~~Clusters G1 with a low fraction of precipitation falling as snow with humid climate show (Clusters 1, 9, 10) high rising limb densities (Fig. 9.b) and (Clusters 5, 7) high rising limb scale parameters (Fig. 9.c). This is because the rising limb density negatively correlates with fraction of precipitation falling as snow (Fig. 9.b), whereas the rising limb scale parameter negatively correlates with aridity (Fig. 9.c). Moreover, these Clusters G1 experience a low value of (Clusters 6, 7) falling limb density (Fig. 9.e). This is because the falling limb density positively correlates with the climate indices (Fig. 9.e).~~

~~As mentioned earlier, Clusters G2 with humid climate and with a high fraction of precipitation falling as snow (Clusters 3, 4) display low values of rising limb density as rising limb density correlates negatively with the fraction of precipitation falling as snow (Fig. 9.b). G2 witnesses higher values of rising limb shape parameter due to its negative correlation with aridity and positive correlation with the fraction of precipitation falling as snow (Fig. 9.d). Furthermore, the Clusters of G2 (Clusters 3, 4) show low values of recession coefficients as they depict a strong negative correlation with the fraction of precipitation falling as snow (Fig. 9.f, g).~~

~~Low values of rising limb scale and shape parameters are noticed for the Clusters 2, 9, 8 (Clusters G3) with arid climate and low fraction of precipitation falling as snow (Fig. 9.c, d) due to its negative correlation with aridity as stated earlier. Cluster 8 experiences the maximum values of falling limb density (Fig. 9.e) where the region witnesses low fraction of snow and arid catchments, due to its strong positive correlates with the aridity.~~

4.2 Influence of Attributes of Climate to Streamflow Indices

The climatic indices indicate a more substantial influence on hydrological signatures than the topographic, soil, land cover, and geological attributes combined (Addor et al., 2018, Stein et al., 2021). Additionally, the findings of Jehn et al. (2020) highlighted that the climate appears to be the most critical factor influencing hydrological behavior in the CAMELS dataset as a whole, and depending on the location, either aridity, snow, or seasonality are most important. Hence, the streamflow indices are then examined in the climate index space (aridity along x-axis and fraction of precipitation falling as snow along the y-axis) to evaluate the main drivers of the catchments. Single dots show the catchments and are colored by their hydrological clusters (Fig. 9.a).

Formatted: Not Highlight

Clusters 5, 6, 7, 1, 10 are characterized by a low fraction of precipitation falling as snow and humid climate, whereas Clusters 3, 4 have humid climate experiencing a high fraction of precipitation falling as snow (Fig. 9.a). Clusters 2, 8, 9 are featured by a low fraction of precipitation falling as snow and arid climate (Fig. 9.a). The three categories mentioned above are referred to as G1, G2, and G3, respectively.

Clusters G1 with a low fraction of precipitation falling as snow with humid climate show (Clusters 1, 9, 10) high rising limb densities (Fig. 9.b) and (Clusters 5, 7) high rising limb scale parameters (Fig. 9.c). This is because the rising limb density negatively correlates with fraction of precipitation falling as snow (Table 2: r = -0.33, Fig. 9.b), whereas the rising limb scale parameter negatively correlates with aridity (Table 2: r = -0.53, Fig. 9.c). Moreover, these Clusters G1 experience a low value of (Clusters 6, 7) falling limb density (Fig. 9.e). This is because the falling limb density positively correlates with the climate indices (Table 2: r = 0.42 for fraction of precipitation falling as snow and r = 0.39 for aridity, Fig. 9.e).

As mentioned earlier, Clusters G2 with humid climate and with a high fraction of precipitation falling as snow (Clusters 3, 4) display low values of rising limb density as rising limb density correlates negatively with the

fraction of precipitation falling as snow (Table 2: r = -0.33, Fig. 9.b). G2 witnesses higher values of rising limb shape parameter due to its negative correlation with aridity (r = -0.16) and positive correlation with the fraction of precipitation falling as snow (Table 2: r = 0.53, Fig. 9.d). Furthermore, the Clusters of G2 (Clusters 3, 4) show low values of recession coefficients as they depict a strong negative correlation with the fraction of precipitation falling as snow (Table 2: upper_r = -0.46, and lower_r = -0.39, Fig. 9.f, g).

Low values of rising limb scale and shape parameters are noticed for the Clusters 2, 9, 8 (Clusters G3) with arid climate and low fraction of precipitation falling as snow (Fig. 9.c, d) due to its negative correlation with aridity as stated earlier. Cluster 8 experiences the maximum values of falling limb density (Fig. 9.e) where the region witnesses low fraction of snow and arid catchments, due to its strong positive correlates with the aridity (r = 0.39).

Formatted: Space Before: 0 pt, After: 8 pt, Widow/Orphan control, Adjust space between Latin and Asian text, Adjust space between Asian text and numbers

Formatted: Font: Not Bold, English (United States)

5 Concluding remarks

Streamflow hydrograph portrays the time distribution of runoff at the point of measurement by a single curve, and the hydrographs are characterized by their time irreversibility property. In this study, the indices related to this characteristic feature are used to study the catchment drivers of streamflow hydrograph. The streamflow indices associated with the time irreversibility of hydrograph open new opportunities to investigate the interaction between topography, soil, climate, vegetation, geology that drive the hydrological behavior of catchments. Moreover, most of the previously presented hydrologic indices are employed only for time-symmetric processes (McMillan, 2021); the importance of the time irreversibility of streamflow is highlighted in this study. The indices associated with rising and falling limbs are primarily correlated to distinct catchment attributes, establishing a relationship between the indices and catchment attributes such as climate, topography, soil, geology, and vegetation to delineate the controlling drivers in corresponding hydrograph sections. A set of streamflow indices with temporal asymmetry for 671 catchments in the United States is presented in this study. The regional variations among catchments over the United States are compared and discussed using the spatial maps of streamflow indices. Such spatial maps of the streamflow indices supplement the hydrometeorological time series and catchment attributes provided by Addor et al. (2017).

~~The study revealed that the rising limb indices such as rising limb density, rising limb shape parameter and rising limb scale parameter correlate positively with vegetation indices. Falling limb density is primarily controlled by climate indices and is negatively correlated with land cover characteristics; the structure of the falling limb density is also closely influenced by mean elevation.~~ The study showed that the rising limb density is mainly governed by the elevation and fraction of precipitation falling as snow. Climate indices, mean elevation, and the fraction of precipitation falling as snow mainly influence falling limb density. In contrast, the aridity and frequency of precipitation drive the rising limb scale parameter. Furthermore, forest fraction, the fraction of precipitation falling as snow, mean slope, mean elevation, sand fraction, and precipitation frequency influence the rising limb shape parameter. Mean elevation, mean slope, clay, the fraction of precipitation falling as snow, forest fraction, and sand fraction all determine recession coefficients. Finally, streamflow indices are studied in the climate index space to isolate the runoff generation's leading drivers. High rising limb densities and rising limb scale parameters are observed in catchments with low precipitation falling as snow and a humid climate. It is observed that the catchments with a humid climate and a high fraction of precipitation falling as snow display low values of rising limb density, high values of the rising limb shape parameter, and low values of recession coefficients. The lowest values of rising limb scale and shape parameters, and the highest values of falling limb density, are seen in

catchments of arid climates and a low fraction of precipitation falling as snow.

In general, the contribution of this work lies in differentiating hydrographs depending on their time irreversibility property and using the corresponding indices to provide an alternative methodology for identifying the drivers of streamflow hydrographs. In the context of large sample hydrology research, the concept of time-irreversibility and the indices associated with it could also be used to describe the drivers at catchment scale. It must be noted that ~~E~~each attribute (e.g., climate vegetation, soil, geology) usually does not exist independently in space but is closely interwoven, resulting in various strongly correlated attributes in a catchment (Jehn et al., 2020; Stein et al., 2021). However, it would be beyond the scope of this paper ~~document~~ to describe all probable relationships between attributes. Keeping this in mind, the main focus of this study was constrained to only identify the controlling attributes of streamflow indices. Another limitation of the work is related with the characterization of recessions used.

Future work may investigate using the inflection point or another recession separation technique to characterize recessions.

Data availability. The CAMELS dataset can be found at https://doi.org/10.5194/hess21-5293-2017 (Addor et al. 2017). The hydrometeorological time series (https://doi.org/10.5065/D6MW2F4D) used in this paper are freely available online.

Competing interests. The authors declare that they have no conflict of interest.

Acknowledgements. We would like to thank all the people who created the CAMELS dataset. We sincerely thank Editor Elena Toth, Dr. Wouter Knoben, and the anonymous reviewer for patiently reviewing the manuscript and offering valuable critical comments to improve the manuscript. Their suggestions have significantly improved the quality of our contribution to this revised manuscript.

The funding received from the Ministry of Earth Sciences (MoES), Government of India, through the project, "Advanced Research in Hydrology and Knowledge Dissemination", Project No.: MOES/PAMC/H&C/41/2013-PC-II, is gratefully acknowledged.

References

Addor, Newman, A. J., Mizukami, N. and Clark, M. P.: The CAMELS data set: catchment attributes and meteorology for large-sample studies, Hydrol. Earth Syst. Sci., 21(10), 5293–5313, doi:10.5194/hess-21-5293-2017, 2017.

Addor, Nearing, G., Prieto, C., Newman, A. J., Le Vine, N. and Clark, M. P.: A Ranking of Hydrological Signatures Based on Their Predictability in Space, Water Resour. Res., 54(11), 8792–8812, doi:10.1029/2018WR022606, 2018.

Addor, N., Do, H. X., Alvarez-Garreton, C., Coxon, G., Fowler, K. and Mendoza, P. A.: Large-sample hydrology: recent progress, guidelines for new datasets and grand challenges, Hydrol. Sci. J., 65(5), 712–725, doi:10.1080/02626667.2019.1683182, 2020.

Alvarez-Garreton, C., Mendoza, P. A., Pablo Boisier, J., Addor, N., Galleguillos, M., Zambrano-Bigiarini, M., Lara, A., Puelma, C., Cortes, G., Garreaud, R., McPhee, J. and Ayala, A.: The CAMELS-CL dataset: Catchment attributes and meteorology for large sample studies-Chile dataset, Hydrol. Earth Syst. Sci., 22(11), 5817–5846, doi:10.5194/hess-22-5817-2018, 2018a.

Alvarez-Garreton, C., Mendoza, P. A., Boisier, J. P., Addor, N., Galleguillos, M., Zambrano-Bigiarini, M., Lara, A., Puelma, C., Cortes, G., Garreaud, R., McPhee, J. and Ayala, A.: The CAMELS-CL dataset: catchment attributes and meteorology for large sample studies – Chile dataset, Hydrol. Earth Syst. Sci., 22(11), 5817–5846, doi:10.5194/hess-22-5817-2018, 2018b.

Arsenault, R., Bazile, R., Ouellet Dallaire, C. and Brissette, F.: CANOPEX: A Canadian hydrometeorological watershed database, Hydrol. Process., 30(15), 2734–2736, doi:10.1002/hyp.10880, 2016.

Berghuijs, W. R., Sivapalan, M., Woods, R. A. and Savenije, H. H. G.: Patterns of similarity of seasonal water balances: A window into streamflow variability over a range of time scales, Water Resour. Res., 50(7), 5638–5661, doi:10.1002/2014WR015692, 2014.

Blöschl, G., Hall, J., Viglione, A., Perdigão, R. A. P., Parajka, J., Merz, B., Lun, D., Arheimer, B., Aronica, G. T., Bilibashi, A., Boháč, M., Bonacci, O., Borga, M., Čanjevac, I., Castellarin, A., Chirico, G. B., Claps, P., Frolova, N., Ganora, D., Gorbachova, L., Gül, A., Hannaford, J., Harrigan, S., Kireeva, M., Kiss, A., Kjeldsen, T. R., Kohnová, S., Koskela, J. J., Ledvinka, O., Macdonald, N., Mavrova-Guirguinova, M., Mediero, L., Merz, R., Molnar, P., Montanari, A., Murphy, C., Osuch, M., Ovcharuk, V., Radevski, I., Salinas, J. L., Sauquet, E., Šraj, M., Szolgay, J., Volpi, E., Wilson, D., Zaimi, K. and Živković, N.: Changing climate both increases and decreases European river floods, Nature, 573(7772), 108–111, doi:10.1038/s41586-019-1495-6, 2019.

Clark, M. P., McMillan, H. K., Collins, D. B. G., Kavetski, D. and Woods, R. A.: Hydrological field data from a modeller's perspective: Part 2: Process-based evaluation of model hypotheses, Hydrol. Process., 25(4), 523–543, doi:10.1002/hyp.7902, 2011.

Coxon, G., Freer, J., Wagener, T., Odoni, N. A. and Clark, M.: Diagnostic evaluation of multiple hypotheses of hydrological behaviour in a limits-of-acceptability framework for 24 UK catchments, Hydrol. Process., 28(25), 6135–6150, doi:10.1002/hyp.10096, 2014.

Coxon, G., Addor, N., Bloomfield, J. P., Freer, J., Fry, M., Hannaford, J., Howden, N. J. K., Lane, R., Lewis, M., Robinson, E. L., Wagener, T. and Woods, R.: CAMELS-GB: hydrometeorological time series and landscape attributes for 671 catchments in Great Britain, Earth Syst. Sci. Data, 12(4), 2459–2483, doi:10.5194/essd-12-2459-2020, 2020.

Do, H. X., Gudmundsson, L., Leonard, M. and Westra, S.: The Global Streamflow Indices and Metadata Archive (GSIM) – Part 1: The production of a daily streamflow archive and metadata, Earth Syst. Sci. Data, 10(2), 765–785, doi:10.5194/essd-10-765-2018, 2018.

Duan, Q., Schaake, J., Andréassian, V., Franks, S., Goteti, G., Gupta, H. V., Gusev, Y. M., Habets, F., Hall, A., Hay, L., Hogue, T., Huang, M., Leavesley, G., Liang, X., Nasonova, O. N., Noilhan, J., Oudin, L., Sorooshian, S., Wagener, T. and Wood, E. F.: Model Parameter Estimation Experiment (MOPEX): An overview of science strategy and major results from the second and third workshops, J. Hydrol., 320(1–2), 3–17, doi:10.1016/j.jhydrol.2005.07.031, 2006.

Ehret, U., Gupta, H. V., Sivapalan, M., Weijs, S. V., Schymanski, S. J., Blöschl, G., Gelfan, A. N., Harman, C., Kleidon, A., Bogaard, T. A., Wang, D., Wagener, T., Scherer, U., Zehe, E., Bierkens, M. F. P., Di Baldassarre, G., Parajka, J., van Beek, L. P. H., van Griensven, A., Westhoff, M. C. and Winsemius, H. C.: Advancing catchment hydrology to deal with predictions under change, Hydrol. Earth Syst. Sci., 18(2), 649–671, doi:10.5194/hess-18-649-2014, 2014.

Ghiggi, G., Humphrey, V., Seneviratne, S. I. and Gudmundsson, L.: GRUN: an observation-based global gridded runoff dataset from 1902 to 2014, Earth Syst. Sci. Data, 11(4), 1655–1674, doi:10.5194/essd-11-1655-2019, 2019.

Gudmundsson, L., Do, H. X., Leonard, M. and Westra, S.: The Global Streamflow Indices and Metadata Archive (GSIM) – Part 2: Quality control, time-series indices and homogeneity assessment, Earth Syst. Sci. Data, 10(2), 787–804, doi:10.5194/essd-10-787-2018, 2018.

Gupta, H. V., Perrin, C., Blöschl, G., Montanari, A., Kumar, R., Clark, M. and Andréassian, V.: Large-sample hydrology: a need to balance depth with breadth, Hydrol. Earth Syst. Sci., 18(2), 463–477, doi:10.5194/hess-18-463-2014, 2014.

Jehn, F. U., Bestian, K., Breuer, L., Kraft, P. and Houska, T.: Using hydrological and climatic catchment clusters to explore drivers of catchment behavior, Hydrol. Earth Syst. Sci., 24(3), 1081–1100, doi:10.5194/hess-24-1081-2020, 2020.

Khrystyuk, B., Gorbachova, L. and Koshkina, O.: The impact of climatic conditions of spring flood formation on hydrograph shape of the Desna River, Meteorol. Hydrol. Water Manag., 5(1), 63–70, doi:10.26491/mhwm/67914, 2017.

Knoben, W. J. M., Woods, R. A. and Freer, J. E.: A Quantitative Hydrological Climate Classification Evaluated With Independent Streamflow Data, Water Resour. Res., 54(7), 5088–5109, doi:10.1029/2018WR022913, 2018.

Koutsoyiannis, D.: Simple stochastic simulation of time irreversible and reversible processes, Hydrol. Sci. J., doi:10.1080/02626667.2019.1705302, 2020.

Kuentz, A., Arheimer, B., Hundecha, Y. and Wagener, T.: Understanding hydrologic variability across Europe through catchment classification, Hydrol. Earth Syst. Sci., 21(6), 2863–2879, doi:10.5194/hess-21-2863-2017, 2017.

Linke, S., Lehner, B., Ouellet Dallaire, C., Ariwi, J., Grill, G., Anand, M., Beames, P., Burchard-Levine, V., Maxwell, S., Moidu, H., Tan, F. and Thieme, M.: Global hydro-environmental sub-basin and river reach characteristics at high spatial resolution, Sci. Data, 6(1), 283, doi:10.1038/s41597-019-0300-6, 2019.

Mathai and Mujumdar, P. P.: Multisite Daily Streamflow Simulation With Time Irreversibility, Water Resour. Res., 55(11), 9334–9350, doi:10.1029/2019WR025058, 2019.

McMillan, H. K.: A review of hydrologic signatures and their applications, WIREs Water, 8(1), 1–23, doi:10.1002/wat2.1499, 2021.

McMillan, H. K., Clark, M. P., Bowden, W. B., Duncan, M. and Woods, R. A.: Hydrological field data from a modeller's perspective: Part 1. Diagnostic tests for model structure, Hydrol. Process., 25(4), 511–522, doi:10.1002/hyp.7841, 2011.

Newman, A. J., Clark, M. P., Sampson, K., Wood, A., Hay, L. E., Bock, A., Viger, R. J., Blodgett, D., Brekke, L., Arnold, J. R., Hopson, T. and Duan, Q.: Development of a large-sample watershed-scale hydrometeorological data set for the contiguous USA: data set characteristics and assessment of regional variability in hydrologic model performance, Hydrol. Earth Syst. Sci., 19(1), 209–223, doi:10.5194/hess-19-209-2015, 2015.

Richter, B. D., Baumgartner, J. V., Powell, J. and Braun, D. P.: A Method for Assessing Hydrologic Alteration within Ecosystems, Conserv. Biol., 10(4), 1163–1174, doi:10.1046/j.1523-1739.1996.10041163.x, 1996.

Roberts, M. C. and Klingeman, P. C.: The influence of landform and precipitation parameters on flood hydrographs, J. Hydrol., 11(4), 393–411, doi:10.1016/0022-1694(70)90004-1, 1970.

Rogers, W. F.: New concept in hydrograph analysis, Water Resour. Res., 8(4), 973–981, doi:10.1029/WR008i004p00973, 1972.

Sawicz, K., Wagener, T., Sivapalan, M., Troch, P. A. and Carrillo, G.: Catchment classification : empirical analysis of hydrologic similarity based on catchment function in the eastern USA, Hydrol. Earth Syst. Sci., 8(3), 2895–2911, doi:10.5194/hess-15-2895-2011, 2011.

Sawicz, K. A., Kelleher, C., Wagener, T., Troch, P., Sivapalan, M. and Carrillo, G.: Characterizing hydrologic change through catchment classification, Hydrol. Earth Syst. Sci., 18(1), 273–285, doi:10.5194/hess-18-273-2014, 2014.

Serinaldi, F. and Kilsby, C. G.: Irreversibility and complex network behavior of stream flow fluctuations, Phys. A Stat. Mech. its Appl., 450, 585–600, doi:10.1016/j.physa.2016.01.043, 2016.

Shamir, E., Imam, B., Morin, E., Gupta, H. V. and Sorooshian, S.: The role of hydrograph indices in parameter estimation of rainfall-runoff models, Hydrol. Process., 19(11), 2187–2207, doi:10.1002/hyp.5676, 2005.

Singh, V. P.: Effect of spatial and temporal variability in rainfall and watershed characteristics on stream flow hydrograph, Hydrol. Process., 11(12), 1649–1669, doi:10.1002/(SICI)1099-1085(19971015)11:12<1649::AID-HYP495>3.0.CO;2-1, 1997.

Stagge, J. H. and Moglen, G. E.: A nonparametric stochastic method for generating daily climate-adjusted streamflows, Water Resour. Res., 49, 6179–6193, doi:10.1002/wrcr.20448, 2013.

Stein, L., Clark, M. P., Knoben, W. J. M., Pianosi, F. and Woods, R. A.: How Do Climate and Catchment Attributes Influence Flood Generating Processes? A Large-Sample Study for 671 Catchments Across the Contiguous USA, Water Resour. Res., 57(4), 1–21, doi:10.1029/2020WR028300, 2021.

Szilagyi, J., Balint, G. and Csik, A.: Hybrid, Markov chain-based model for daily streamflow generation at multiple catchment sites, J. Hydrol. Eng., 11(3), 245–256, 2006.

Formatted: No bullets or numbering